2.8 SEASONAL HEAT STORAGE AND ADVECTION IN THE CALIFORNIA CURRENT

Kathleen A. Edwards and Kathryn A. Kelly*
University of Washington, Seattle, Washington

1. INTRODUCTION

One role of eastern boundary currents in the coupled climate system is to uptake large amounts of heat from the atmosphere. In the Josey et al. (1998) climatology, the greatest net heat flux into the ocean in the northern subtropical latitudes occurs in the California Current (CC) region, where sea surface temperature (SST) remains cool due to advection of Subarctic Water from the north and to wind-driven upwelling of subsurface water. The goal of the current work is to determine how heat is exchanged, advected, and stored in the CC region on seasonal timescales. The seasonal cycle accounts for ~20% of the variance of oceanic heat content. As well, focusing on the seasonal timescale allows heat budget terms to be estimated from datasets of different time coverage and resolution.

2. METHODS

A seasonal heat budget of the upper ocean is estimated along a shiptrack which crosses the CC region (Fig. 1). By combining satellite and in situ data, we consider the relative importance of the budget terms in the three subregions identified by Lynn and Simpson (1987): the CC itself, a transitional region, and an offshore region.

The heat content is the vertically averaged temperature from the XBT profiles to a depth, *h*, of 500 m, assumed to be deep enough that contribution of vertical motions and heat fluxes at *h* can be neglected. To reduce the noise due to deep motions, the temperature profiles are normalized to the local temporal mean at *h*, as was done in Moisan and Niiler (1998). Advection of heat is attributed to Ekman transport, derived from gridded scatterometer wind stress downloaded from the Centre ERS d'Archivage et de Traitement, and to geostrophic transport of heat. Surface geostrophic velocities were derived from the slope of sea surface height (SSH) from TOPEX/POSEIDON. SSH anomalies were smoothed by Dr. Michael Schlax as described in Schlax et al. (1992), to which was added the mean SSH from Kelly et al. (1998). Gradients of SST were estimated from Pathfinder AVHRR data provided by NASA/JPL PODAAC. It was assumed that the depth-integrated geostrophic transport is proportional to the product of *h* and the surface geostrophic heat transport.

Transport of heat horizontally by eddies cannot be resolved in time. Vertical mixing or isotherm heaving at depth *h* is neglected as well. After a comparison of the performance of various flux products in the budget (Edwards and Kelly, 2004), the Josey et al. (1998) climatology was selected, except for shortwave flux which comes from ISCCP within 500 km of the coast (International Satellite Cloud Climatology Project; Gupta et al. 1999). Each budget term is interpolated to 100-km spacing along the track before two annual harmonics are fit to it.

3. RESULTS

The terms of the heat budget are shown in Fig. 2. Offshore, the heat storage rate (Fig. 2a) resembles the net heat flux (Fig. 2b), as found by Moisan and Niiler (1998). Within ~500 km of shore, however, the phase of the heat storage rate is offset from that of the net heat flux, so that its maximum occurs earlier in the year towards the coast. Heat advection (Fig. 2b and c) is greatest when net heat flux is maximum, reducing the seasonal cycle of heat storage rate and shifting the phase to earlier in the year. The Ekman heat transport (Fig. 2b) is only ~40% as big as the geostrophic component. The geostrophic and Ekman transports are dominated by their alongshore and cross-shore components respectively.

The seasonal sequence of events affecting the heat budget is overlaid on Fig. 2. The cycle begins with the spring transition of winds to upwelling-favorable. The heavy line in Fig. 2b encloses seasonal equatorwards wind stress exceeding 0.02 N m^{-2}. Maximum heat loss due to Ekman transport occurs within the region of strong equatorwards winds. Compared the width of the CC overlaid on Fig. 2c, the wind forcing is applied over a greater crossshore extent. The cross-shore correlation scale of alongshore wind stress with coastal values is ~1500 km from both scatterometer data and ECMWF model output, with little change by season, while that of alongshore velocity from TOPEX/POSEIDON is ~500 km, a typical width of the CC. Further, the oceanic response occurs over a slower timescale than that of the onset of the winds. Following the transition to upwelling favorable winds, the CC widens ~2 cm s^{-1} during the summer to a maximum width of 500 km in fall, followed by a wintertime collapse in width. Inside the widening CC, heat is lost due to geostrophic advection, especially by the alongshore component. The width of the CC was defined in two ways, with nearly identical results. The width shown in Fig. 2c is based on equatorwards velocity exceeding 0.04 ms^{-1} obtained from TOPEX/POSEIDON. A seasonal cycle fit to this width with the annual mean included is shown by the heavy line. The second definition of width is based on the strong SST front at the offshore edge of the CC. The offshore distance at which the SST gradient from AVHRR first exceeds 10^{-5} ^{o}C km^{-1} was fit by a seasonal cycle, and nearly overlies the width shown.

The greatest crossshore scale affecting the heat budget is that of net heat flux; its correlation with coastal values exceeds the 1800-km section of the shiptrack, reflecting the zonal uniformity of shortwave forcing. However, the net heat flux does intensify towards the coast where cloud cover thins (Fig. 2d). The heavy line is a seasonal fit to the crossshore extent of the 70% cloudiness threshold from ISCCP, with the annual mean included. Inshore of the line, cloud cover is less than offshore. As was found in Nelson and Husby (1983), cloud clearing occurs over the widest crossshore distance in summer, permitting more shortwave heat flux to enter the ocean. Because net heat flux is dominated by shortwave, its seasonal amplitude increases towards shore as well.

As Fig. 3 shows, the misfit between the satellite-derived forcing terms and the heat storage rate is 25-50 W m^{-2}, or 50-105% of the seasonal amplitude. This misfit (shaded) is primarily due to the phase offset between the forcing terms and

* *Corresponding author address:* Kathleen A. Edwards, Applied Physics Laboratory, Univ. of Washington, Seattle, WA 98105-6698; e-mail: edwards@apl.washington.edu.

the heat storage rate, since the amplitudes are relatively close. From 200-400 km offshore, the forcing terms lag by 15-50 days. Further offshore, where the influence of currents is less, the forcing terms lead by 20-35 days. This error, which persisted when different net flux and heat content products were tested, likely represents the terms missing from our heat budget, such as the mixing of heat across the base of the integration (h = -500m).

Having established a heat budget and evaluated different flux products within it, we next seek better understanding of the advection terms. To identify which transport events dominate the advection of heat over the course of the year, Fig. 4 separates the alongshore geostrophic heat transport, which is the largest component of advection, into different combinations of flow direction and SST gradient. Heat loss (gain) occurs as relatively cold (warm) water moves across the shiptrack. Results are averaged over the nearest 500 km to the coast, where most transport occurs. The satellite-based transport estimates are binned by 45-day intervals of day of year (unlike the previous figures, in which a seasonal cycle is fit). Within each time bin, the heat advected by a given combination of velocity and temperature gradient is divided by the total advected heat to give the fractional contribution, which can be read off the y-axis. The probability of a given combination is the number of times it occurs divided by the total number of events, and is indicated by the marker size. To help identify water mass sources, the 5-m "spiciness" (Flament et al. 2002), or relative saltiness and warmth of the water, was derived from the ECCO-2 model (Fukimori et al. 1999) and interpolated onto the time of the satellite heat transport estimates, with the temporal and spatial mean removed. Marker color indicates the spiciness anomaly associated with that each of event for each time bin.

The alongshore geostrophic heat transport is dominated by heat loss due to equatorwards flow of relatively cold, fresh water (circles), characteristic of the cool, fresh Pacific Subarctic influence on the equatorwards CC. Year-round, these events have the greatest probability of occurrence. In spring, events of poleward warm, salty flow offset the CC advection, causing a heat gain. These infrequent events are associated either weak or polewards wind stress, such as would be due to storms. In summer through fall, heat is also gained by infrequent events of relatively warm equatorwards flow, which is saltier than the Pacific Subarctic water.

The seasonal heat budget presented here is depth-averaged to 500 m. We next seek to understand where heat is stored within the water column. Fig. 5 presents vertical profiles of the phase and amplitude of the seasonal temperature anomaly at different distances from the coast. At each depth, a marker is placed at the time of greatest seasonal temperature anomaly for the annual (circle) and semiannual (square) harmonic. Only the second (later) maximum in the semiannual is shown. Depths with the largest amplitude of temperature, indicated by larger marker size, have the greatest influence on the seasonal cycle of heat content, which is the vertical integral of temperature.

Everywhere, the amplitude of temperature is greatest within the surface layer (shaded), defined to contain waters warmer than the coldest historical seasonal temperature at the surface. In the mixed layer (solid line) near the ocean's surface, the phase of temperature is set by the maximum in heating from the atmosphere, and the amplitude is greater than elsewhere in the water column. Beneath the mixed layer, the phase transitions smoothly with depth through the surface layer to match the phase of the waters below, while amplitude decreases. Deeper yet in the permanent thermocline, the seasonal cycle is weak and homogeneous with depth, or non-existent.

While the features described above characterize all the profiles, differences are found between coastal and offshore profiles. In the coastal region (0-500 km), the seasonal cycle in the mixed layer is weaker relative to offshore due to heat removal by advection. In addition, the annual harmonic is continuously present from the ocean surface to 300-400 m depth, which is deeper than the ~100-m ventilation depth of the surface layer. This is due to coastal upwelling of mid-depth waters, visible as an upward perturbation in the isotherm defining the surface layer depth (shaded). One consequence of upwelling is that the temperature maximum at depth in the surface layer leads the mixed layer maximum. Cooling due to upwelling is strongest in summertime at 100 km from the coast, moving later in the year with distance from the coast.

Further offshore (600 km and greater), the mid-depth upwelling signal is not present. As the mixed layer deepens in fall and winter, the temperature maximum at depth occurs later than the surface forcing. A strong seasonal cycle is confined to a surface layer of ~150 m depth. A weak secondary seasonal cycle of O(0.1^{o}C) occurs at depths of 400 m and below. Moving offshore, the timing of this maximum shifts later in the year at about 2.5 cm s^{-1}.

4. SUMMARY

A seasonal heat budget has been developed from XBT data, satellite data and global flux products. The onset of upwelling winds and moderate heat loss by Ekman transport is followed by crossshore growth of the CC and heat loss due to alongshore advection of cold water. Oceanic advection causes crossshore variability of the heat storage rate within ~500 km of the coast. Offshore, the local balance identified by Moisan and Niiler (1998) holds. As the CC grows crossshore, it alters the phase of the heat storage rate through advective removal of heat. Kelly et al. (1993) showed that the crossshore widening of the CC occurs at speeds consistent with an Ekman pumping response to the crossshore pattern of wind stress curl. Within the water column, heat propagates downwards over the summer and fall as the mixed layer deepens.

5. REFERENCES

Edwards and Kelly, 2004: Seasonal budget of the California Current from satellite and in situ data. Proc. of AMS Annual Meeting, Seattle, WA.

Flament, P., 2002: A state variable for characterizing water masses and their diffusive stability: Spiciness. *Progr. Oceanog.*, 54, 493-501.

Fukumori, I., R. Raghunath, L. Fu, and Y. Chao, 1999: Assimilation of TOPEX/POSEIDON data into a global ocean circulation model: How good are the results? *J. Geophys. Res.*, 104, 25,647-25,665.

Gupta, S. K., N. A. Ritchey, A. C. Wilber, C. H. Whitlock, G. G. Gibson, and P. W. Stackhouse, 1999: A climatology of surface radiation budget derived from satellite data. *J. Clim.*, 12., 2691-2710.

Josey, S. A., E. C. Kent and P. K. Taylor, 1998: The Southampton Oceanography Centre (SOC) Ocean - Atmosphere Heat, Momentum and Freshwater Flux Atlas. Southampton Oceanography Centre Report, 6, 30 pp. plus figs.

Kelly, K.A., R. C. Beardsley, R. Limeburner, K. H. Brink, J. D. Paduan, and T.K. Chereskin, 1998: Variability of the near-surface eddy kinetic energy in the California Current based on

altimeter, drifter, and moored current data. *J. Geophys. Res.*, 103, 13,067-13,083.

Kelly, K. A., M. J. Caruso, and J. A. Austin, 1993: Wind-forced variations in sea surface height in the northeast Pacific Ocean. *J. Phys. Oc.*, 23, 2393-2411.

Lynn, R. J. and J. J. Simpson, 1987: The California Current system: The seasonal variability of its physical characteristics. *J. Geophys. Res.*, 92, 12947-12966.

Moisan, J. R., and P. P. Niiler, 1998: The seasonal heat budget of the North Pacific: Net heat flux and heat storage rates (1950-1990). *J. Phys. Oc.*, 28, 401-421.

Nelson, C. S., and D. M. Husby, 1983: Climatology of surface heat fluxes over the California current region. *NOAA Technical Report*, 763(NMFS SSRF-763).

Schlax, M. G., and D. B. Chelton, 1992: Frequency domain diagnostics for linear smoothers. *J. Amer. Stat. Assoc.*, 87, 1070-1081.

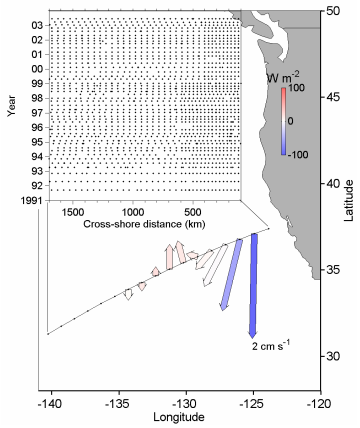

Figure 1: (Inset) Time series of XBT drop locations along the San Francisco to Hawaii ship track. Arrows indicate seasonal surface velocity in late August, when heat loss due to geostrophic advection (color scale) is greatest.

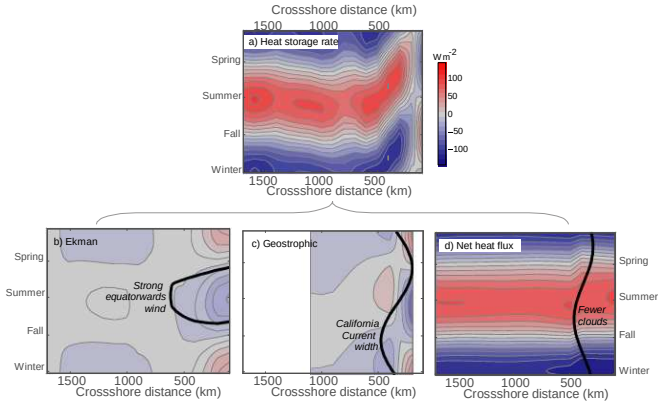

Figure 2: Terms of seasonal heat budget. a) Heat storage rate. b) Ekman transport of heat; strong equatorwards winds occur within heavy contour. c) Geostrophic heat transport; width of CC. d) Net heat flux; greater likelihood of cloud clearing occurs inshore of heavy contour.

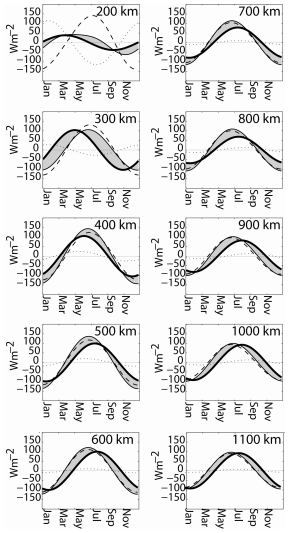

Figure 3: Seasonal fit to heat storage rate (heavy solid line), net heat flux (dashed), and advection (dotted). The misfit between the heat content and the sum of forcing terms (light solid line) is shaded.

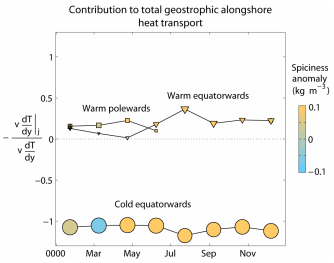

Figure 4: Fractional contribution of different flow events to alongshore geostrophic heat transport: relatively cold equatorwards flow, warm equatorward flow, and warm poleward flow. Relatively cold poleward flow not observed. Marker size scales with probability of occurrence; color indicates spiciness anomaly from ECC0-2 model output. Data averaged over 500 km from coast.

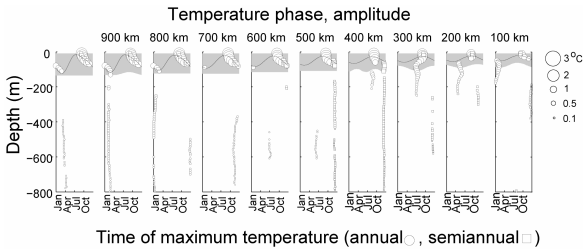

Figure 5: Depth profiles of annual (circles) and semiannual (squares) cycle of temperature, at different distances from shore. Markers are plotted at time of maximum temperature anomaly. Marker area increases with amplitude (scale on right). Surface layer depth is shaded. Mixed layer depth indicated by black line.